Global Spatial Distribution of Hack's Law Exponent on Mars Consistent with Early Arid Climate

W. Luo[1], A. D. Howard[2], R. A. Craddock[3], E. A. Oliveira[4], R. S. Pires[4]

[1]Northern Illinois University, DeKalb, IL, USA

[2]Planetary Science Institute, Tucson, AZ, USA

[3]Smithsonian Institution, Washington, DC, USA

[4]University of Fortaleza, Fortaleza, Ceará, Brazil

Corresponding author: Wei Luo (wluo@niu.edu)

Key Points:

- A parameter free Invasion Percolation Based Algorithm is adapted to delineate watersheds draining to mapped valley networks on Mars.
- The mean and standard deviation of Hack's Law exponent on Mars are similar to those of arid regions on Earth, suggesting similar climate.
- Spatial statistics of Hack's Law exponent show clustered distribution, likely caused by regional topography and/or later modification.

Abstract

Widespread valley networks (VNs) on Mars and other evidence point to an early warm and wet climate. However, ongoing debates still exist about VN's formation processes and associated climatic conditions. The power law relationship between basin length and area (Hack's Law) can be diagnostic of different fluvial processes related to climatic conditions. Past studies of Hack's Law on Mars at local sites have produced inconclusive results. Here we used a parameter-free method to delineate watersheds globally on Mars based on mapped VNs and extracted their Hack's Law exponent (h). The majority of h values on Mars are similar to those in arid areas on Earth, suggesting similar runoff processes and arid conditions for VN formation on early Mars. Statistical analyses show that the spatial distribution of h on Mars is not random, but with a few clustered high and low values, likely controlled by local conditions (e.g., regional topographic slope).

Plain Language Summary

Valley networks on Mars are river-valley-like features distributed primarily across the ancient cratered highland terrains. There are still debates on how they were formed and under what climatic conditions. We adapted an algorithm that only requires mapped valley networks and topography data as input to extract drainage basins on Mars and then examined the relationship between valley network length and drainage area (known as Hack's Law). We also replicated the same analysis to Earth for comparison. We found Hack's Law relationship for the majority of Martian watersheds to be similar to those of terrestrial watersheds formed in arid regions. The widespread distribution of Hack's Law relation on Mars similar to those of arid regions on Earth is consistent with Martian valley network formation by runoff erosion in an arid climate.

1 Introduction

Valley networks (VNs) on Mars are river-valley-like features distributed primarily across the ancient cratered terrains. These features are widely interpreted as a record of past fluvial erosion, implying prolonged liquid water that flowed across the surface in a warm and wet early climate (e.g., Ansan & Mangold, 2013; Craddock & Howard, 2002; Hynek & Phillips, 2003; Luo & Stepinski, 2009; Mangold et al., 2004; Ramirez & Craddock, 2018). However, some climate models have difficulties in producing the necessary warm and wet conditions because Mars is in an orbit farther away from the Sun, thus it receives only about 43% of the solar energy that Earth does. In addition, the Sun's luminosity 3.8 billion years ago (when most of the VNs were believed to be formed) was only ~70% of its present value (Gough, 1981). This has led to many debates about VN's formation processes and early Mars climatic conditions. For example, it may have been that the early climate of Mars was only episodically warm and wet created by brief and strong volcanic activity and associated outgassing of greenhouse gasses and aerosols (Halevy & Head, 2014); or that VNs were formed by groundwater sapping associated with magma intrusion and hydrothermal activities, thus not requiring continuous warm and wet conditions (Gulick, 1998); VNs could also be created during short-lived episodes of top-down melting of thick cold-based ice on the equatorial highlands (Fastook & Head, 2015; Forget et al., 2013; Wordsworth, 2016; Wordsworth et al., 2013) or localized basal melting and erosion by subglacial flows (e.g., Buffo et al., 2022; Grau Galofre et al., 2020, 2022). Scientists are still debating which climatic scenario is correct and whether runoff not involving rainfall can create the observed VNs (e.g., Baker et al., 2015; Ehlmann et al., 2011; Ramirez et al., 2020; Turbet & Forget, 2019).

Quantitative morphometric analysis of the landforms at basin scales can provide valuable information regarding past processes and climatic conditions and thus help test them. Hack's Law exponent is one such morphometric measure. Here we report a global scale analysis of Hack's Law exponent on Mars in comparison with terrestrial analysis and draw the implications for early Mars climate.

1.1 Previous Studies of Hack's Law Exponent on Earth and Mars

Hack's Law is an empirical power law relationship between drainage basin area and the length of the main stream channel (Hack, 1957):

$$L = kA^h \quad (1)$$

where L is the length from a locality on a stream to the drainage divide measured along the channel of the longest stream above that locality; A is the area of the basin that drain to the same locality; h is the Hack's exponent; and k is a constant. Theoretically, for self-similar networks, h = 0.5 (Dodds & Rothman, 2000). In general, h~0.5–0.6 are expected for fluvial systems (e.g., Hack, 1957; Penido et al., 2013; Rigon et al., 1993), implying that watersheds are slightly elongated downstream. Yi et al. (2018) found that the Hack's exponent is also correlated with climate (aridity). In arid areas, h is roughly 0.5, whereas in humid areas h is approximately 0.6. This is attributed to the groundwater involvement in the valley development in humid regions, which decreases transmission loses and allows channels to flow slightly longer distances (Yi et al., 2018).

A number of studies have examined the Hack's Law exponent for selected VN systems or basins on Mars. For example, Som et al. (2009) examined 10 large VN systems and found that h ranges from 0.47 to 19.2, in contrast to the narrower terrestrial range of 0.5-0.6. Caprarelli & Wang (2012) obtained h value of 1.02 for Evros Vallis. Penido et al. (2013) studied a number of selected

small VN systems based on HRSC DEM data and found h = 0.56 ~ 0.89 with a median value of 0.74. Ansan and Mangold (2013) analyzed 13 selected basins and found h = 0.47 ~ 0.78. Although Mars has a lower gravity than Earth, Mars is also slightly more efficient at transporting sand-sized particles, thus Hack's Law should hold for Mars with comparable h values, similar to scaling relationship between channel width and drainage area (Som et al., 2009). However, these previous studies have only looked at various selected areas. We are not aware of any a global comprehensive study on the spatial distribution of Hack's Law exponent on Mars. Our study intends to fill this gap.

2 Materials and Methods

2.1 Data

For the conterminous US on Earth, we used the void filled digital elevation model (DEM) of HydroSHEDS core dataset (https://www.hydrosheds.org/hydrosheds-core-downloads) at 15 and 3 arc second resolutions, which were resampled at 450 m/pixel and 200 m/pixel, respectively. This provides topographic data equivalent to Mars DEM data. For the purpose of extracting watershed boundary (see Section 2.2), we used a dataset of US major streams from the US National Weather Service (https://www.weather.gov/gis/Rivers), because this dataset contains the USGS hydrologic unit level 6 (HUC6) code of the major streams. This allowed us to extract watershed boundary roughly equivalent to the HUC6 basins (see Section 2.2). This level of watershed information provides a reasonable size and resolution for a continental scale analysis. This level of detail has also been used in other similar studies (e.g., Yi et al., 2018). For global Earth analysis, we used level 6 HydroBASINS data (https://www.hydrosheds.org/products/hydrobasins). We also utilized the Global Aridity Index (AI) and the Potential Evapotranspiration Climate Database (Trabucco & Zomer, 2022) for Earth climate information. For Mars, we used MOLA DEM at 463 m/pixel resolution (Smith et al., 2001) and the HRSC and MOLA Blended Digital Elevation Model at 200 m/pixel (Fergason et al., 2018). We also used the mapped VNs (Matsubara et al., 2013) while delineating the watershed boundaries using the IPBA algorithm as described below.

2.2 Watershed delineation

Delineating the watershed boundary is the first step for deriving Hack's law exponent. For terrestrial analysis, the standard technique is to use a flow-based method to extract watershed boundaries from a DEM that is usually implemented in some form of GIS software. Typically this involves filling the depressions in the DEM to make it drainable, deriving flow direction based on the steepest descent (e.g., the D8 algorithm), and finding the flow accumulation along flow direction as the cumulative number of upstream cells flowing into each cell. The flow accumulation above a certain threshold defines the VN, and cells draining into each VN are grouped as the watershed (e.g., O'Callaghan & Mark, 1984). However, the flow-based method is designed for processing Earth data, and it is notoriously difficult to apply to Mars due to the disruptions and fragmentations of topography by impact cratering that post-date VN formation. The arbitrarily chosen flow accumulation threshold can easily result in stream networks that are over- or under-extracted, and tedious human intervention is often necessary to remove spurious results (Ansan & Mangold, 2013; Mest et al., 2010; Stepinski & Coradetti, 2004).

Alternatively, the Invasion Percolation-Based Algorithm (IPBA) is a parameter-free algorithm that is robust and efficient (Fehr et al., 2009; Oliveira et al., 2019; Wilkinson & Willemsen, 1983) and well suited for cratered topography. Invasion Percolation (IP) was originally designed to simulate one fluid displacing another from a porous medium under the action of capillary forces (Wilkinson & Willemsen, 1983), but it has been successfully applied to delineate watershed (Fehr et al., 2009; Oliveira et al., 2019). This works in principle because IP can be applied to any process which proceeds along a path of least resistance (Wilkinson & Willemsen, 1983), and the fluvial processes that form watersheds also follow the least resistance path (i.e., the steepest descent downhill). We adapted this algorithm for the purpose of delineating watershed draining to mapped VNs (or streams) by first converting the VN/stream vector lines into raster cells so that each of the converted VN/stream raster cell serve as a sink in IPBA. Given a regular elevation grid (DEM) and a set of sinks S (streams/valleys) (Fig. 1a & 1b), the IPBA sequentially applies the traditional IP algorithm over all cells of the grid, starting from a source cell (i.e., a seed cell) to form an invaded cluster (Fig. 1c). The growth dynamics iteratively add *the lowest of its neighboring cells* to the cluster (i.e., growing the cluster by invading the surrounding cells, 4-connected neighborhood adopted here). The invaded cluster grows until it reaches a sink cell (or a cell that was once part of an invaded cluster in previous IPBA iterations) and the invaded cluster is labeled with the ID of the sink cell (or the ID of the cluster already labeled). The clusters draining to the same VN/stream are grouped to form the watershed of that VN/stream (same color in Fig. 1d). Finally, the contact edge between different watersheds (different colors) is then marked as the watershed boundary between them (Fig. 1e). As shown in Fig. 1, IPBA is a fundamentally different from flow-based algorithm. IBPA does require mapped VN as input and finds the watershed boundary by IP until the invasion cluster reaches a sink cell, thus avoids the preprocessing (filling) to deal with local depressions. The python code for this version of IPBA is available on GitHub (https://github.com/erneson/IPBA).

An intuitive way to understand the idea behind the IPBA is to consider a simple flooding model (Fehr et al., 2009). The model gradually increases the flood level at each iteration, so that cells under water form unlabeled clusters and grow over the landscape. The unlabeled clusters are only labeled when they touch a sink cell. These labels stand until the end of the process. The watershed boundary is defined by the interface line between two labeled clusters. The flooding model is a slightly adjusted version of a well-known watershed algorithm for image segmentation (Vincent & Soille, 1991). It was already shown that the IPBA is mathematically equivalent to the flooding model, but IPBA is more time efficient (Fehr et al., 2009), which is why we adopted IPBA here.

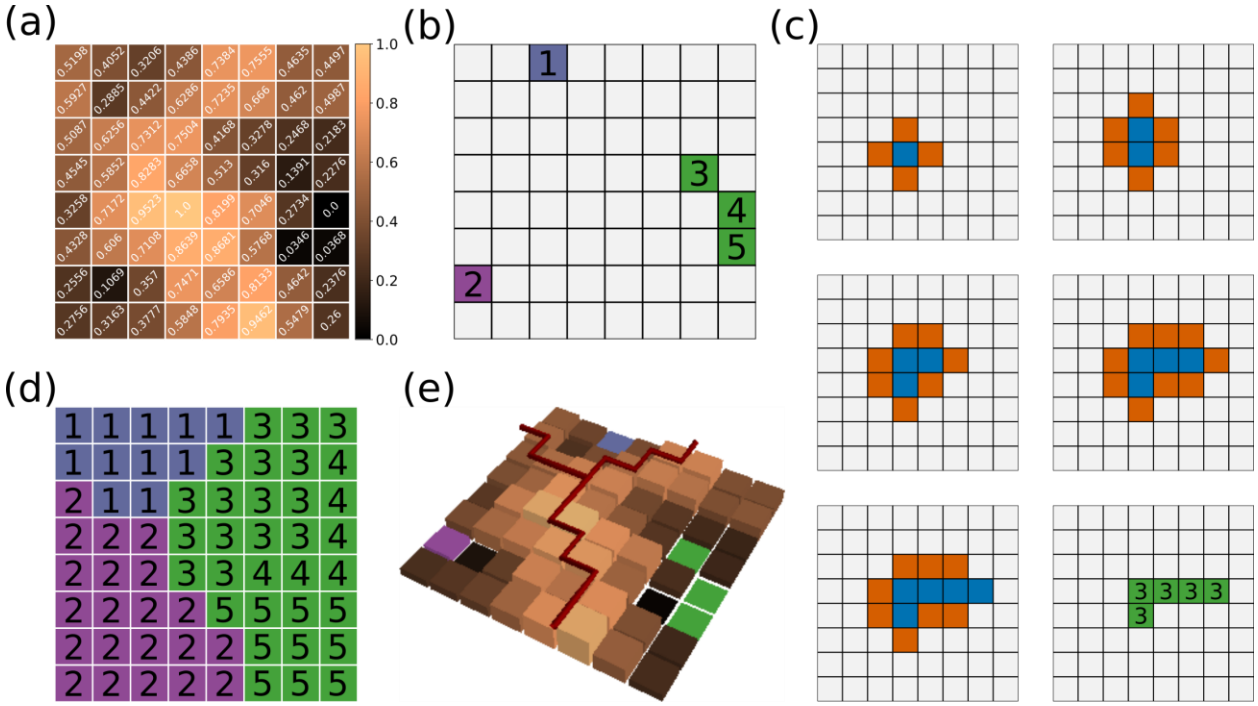

Figure 1. Illustration of the Invasion Percolation Based Algorithm (IPBA). (a) Artificial landscape colored according to the elevation of the cells. (b) Sink cells, same color indicating same VN. (c) Applying the traditional Invasion Percolation (IP) algorithm, starting from a source cell (in blue) and invading neighboring cells (in orange). The invasion process iteratively adds *the lowest of its neighbors* (see elevation in (a)) to the cluster (changing to blue) until reaching a sink cell (the one labeled as 3 and belonged to the green VN). The invaded cluster for that source cell is composed of all blue cells. (d) Result of successive iterations of the IPBA for all cells in the landscape, after joining the invaded clusters that belong to the same VN shown in (b). (e) The artificial landscape in 3D and the watershed boundary (red line) formed by the interface of cells belonging to different VNs.

Although various watershed boundaries exist for Earth, to make fair comparison of the analyses of Hack's law exponents for Earth (US) and Mars, we extracted watersheds for both planets using the same IPBA method as described above. The only inputs required for IPBA are valley/stream lines and a DEM. For Earth we used US major streams and 450 m DEM; for Mars, we used mapped VN and the 463 m MOLA DEM (see Section 2.1). The results for the US are shown in Fig. S1(a). In general, the IPBA extracted watershed boundaries coincide with the independently derived USGS HUC6 boundary very well with a few exceptions, such as around the Great Lakes area, at the southern border with Mexico, and some minor differences in the interior. These exceptions may be caused by less well defined ridge lines in flat area, poor local quality of input stream data or DEM data. Overall, the resulting watershed boundaries are consistent with the input streams and follow along the topographic ridge lines. We also tested the algorithm on different resolution data of the same area (30 m, 90 m, 250 m) on Earth and although there are minor differences between the various resolutions, usually by only a few pixels, the identified watershed boundary always follow the topographic ridge lines in the respective data. The result of applying IPBA to Mars is shown in Fig. S1(b). The watershed boundaries also generally follow topographic ridge lines and are consistent with the mapped VNs.

2.3 Extracting Hack's Law exponent

Although Hack's law relates basin length and area (Eq. (1)), the exponent *h* is strongly influenced by the shape of the basin (Fig. S2). So to extract Hack's law exponent we selected conformal map projections (Contiguous Lambert Conformal Conic projection for US and Mercator Projection for Mars), which by definition preserve the shapes of basins. We also corrected the distortion in length and area in conformal projection, although this correction may not be needed for determining the exponent (see notes under Fig. S2). We first clipped the 200 m DEM using the watershed boundary, one watershed at a time, then used the standard flow-based method to derive flow accumulation in each cell (i.e., *A* in Eq. (1)) and longest upslope distance from each cell along the flow path to the top of the drainage divide (*L* in Eq. (1)) using the flow accumulation and flow length tools, respectively, in ArcGIS Pro. Next, the optimize.curve_fit function in SciPy was used to fit the power law relationship to obtain the exponent *h* in Eq. (1). An example of watershed and Hack's Law exponent is shown in Fig. S3.

3 Results

3.1 Terrestrial

To provide context and aid in interpreting our results for Mars, we extracted the Hack's Law exponent for the conterminous US as described above. The results from this effort are shown in Table S1 and Fig. 2. Our results, although slightly different in values, are generally consistent with those of Yi et al. (2018). The *h* values are generally higher in humid regions (0.54) than those in arid ones (0.50) (Table S1, Fig. 2a & 2b). Although there is scatter in the AI vs. *h* plot (Fig. S4), statistic t-test show that the difference of Hack's law exponents between the humid (AI > 0.65) and arid (AI ≤ 02) regions are highly statistically significant ($p<0.0001$, one-tail, Table S2). Analysis of the whole Earth produced result very similar to that of the US (Fig. S5 and Table S3).

In order to examine if the spatial distribution of *h* is random or clustered and to explore possible causes of the patterns, we conducted further spatial analyses. We excluded basins that have poor fitting for Hack's law exponent ($r^2 < 0.75$), because the *h* values with low r^2 are less reliable. There are 6 such basins, which occur mostly in flat areas, including one draining into Lake Superior and 5 small basins in the Mississippi delta (Fig. 2d and Table S1). We first conducted spatial autocorrelation analysis (Global Moran's I) of *h* over conterminous US using ArcGIS Pro software (ESRI, n.d.-a) (see Supplement Material 2.1). The null hypothesis is that the spatial distribution of *h* is random, i.e., *h* is spatially uncorrelated. The analysis generated a Moran's Index of 0.2297, a z-score of 7.733 and a p-value of <0.0001, which means that the distribution is highly clustered and the null hypothesis can be safely rejected. This makes sense, because we know on Earth fluvial processes are primarily responsible for the formation of drainage systems.

We next conducted Optimized Hot Spot Analysis (ESRI, n.d.-b). This tool identifies statistically significant spatial clusters of high values (hot spots) and low values (cold spots) using optimal settings (e.g., scale) derived from the data that will yield optimal hot spot results (ESRI, n.d.-b) (see Supplement Material 2.2). *Please note that the hot/cold here simply means spatially*

clustered high/low values and does not imply climate condition. The result is shown in Fig. 2d. The hotspot in the north is located at the Wyoming-Dakota border around the Black Hills area and the one in the south is located in the area transitioning from Great Plains to Central Lowland area (Hunt, 1967). Both are characterized by some parallel to sub-parallel drainage systems. The south hotspot area is largely fed from the Rockies crossing older ~Cretaceous sedimentary platform derived from the Rockies and there was a change from deposition in the Great Plains in the late Mesozoic to erosion in the later Cenozoic. The hotspots (high *h* values) are likely caused by fluvial erosion that elongated the watershed in the downslope direction of the regional slope. The cold spots are generally located at the Basin and Range Province and Colorado Plateau (Hunt, 1967), a generally very arid region (cf Fig. 2b). The cold spots (low *h* values) are related to the arid climate and/or structure control of basin and range. The descriptive statistics of *h* in these hot/cold spots are shown in Table S1.

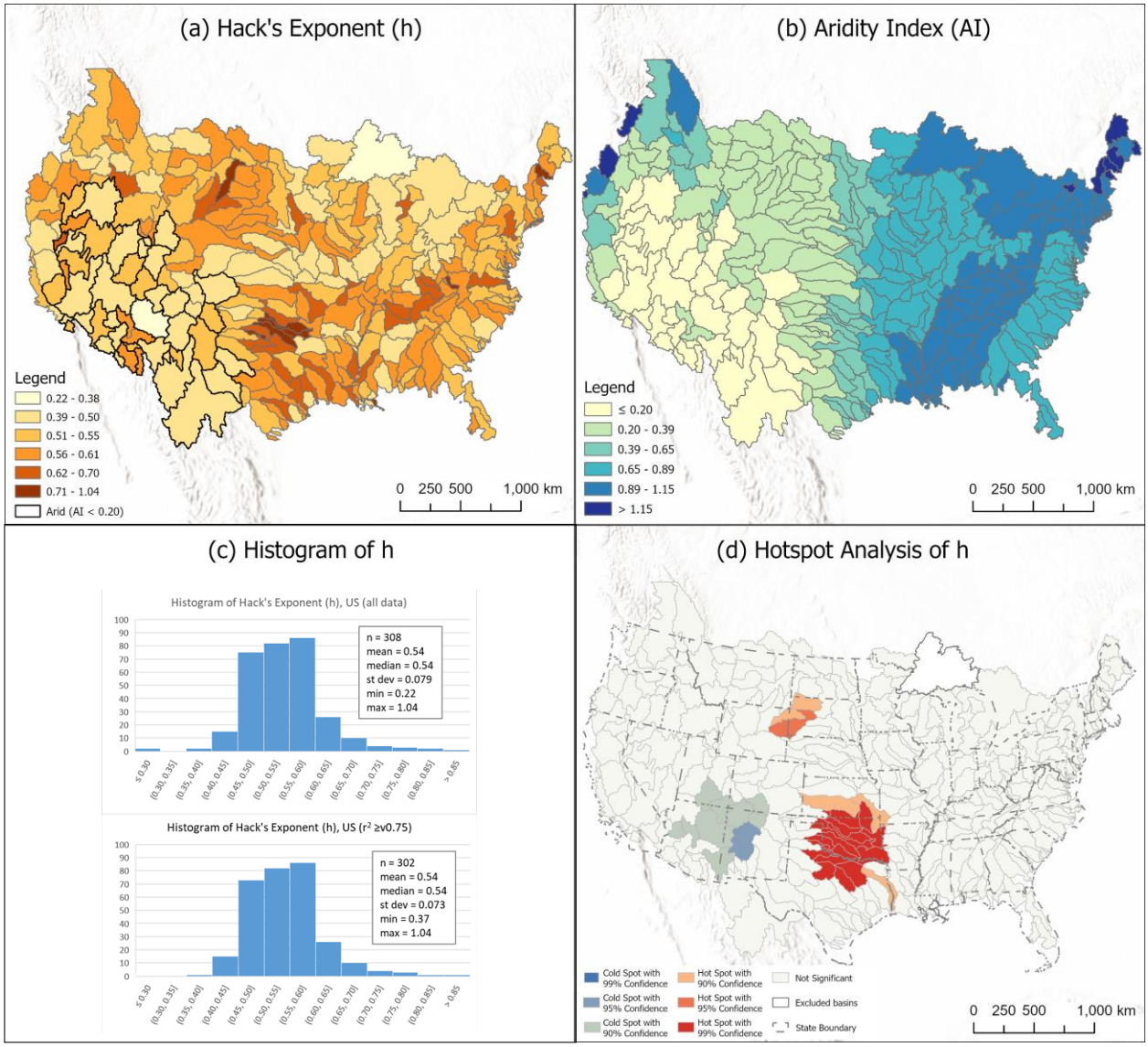

Figure 2. (a) Distribution of Hack's Law exponent *h* of conterminous US (note: *h* is derived from 200 m resolution DEM). Arid area (bold outline) is defined as basins with median AI less than 0.20 (UNEP, 1997). (b) Spatial distribution of median value of AI by watershed of US. (c) Histogram of *h* for conterminous US (top: all watersheds included; bottom: only those with $r^2 \geq 0.75$). (d) Hotspot Analysis of *h*.

3.2 Mars

Fig. 3a shows the spatial distribution of *h* of the 2562 watersheds on Mars that are not on the edge of the DEM grid, because those on the edge have artificial straight boundaries, which could result in inaccurate *h*. Fig. 3b shows the histogram of *h* of the 2562 watersheds. The histogram is roughly normally distributed, ranging from 0.054 (min) to 2.1 (max) with a mean value of 0.49 and standard deviation of 0.086 (Table S1). The minimum and maximum values are more extreme than their terrestrial counterparts; however, the frequency of these extreme values are low. After further excluding the basins with poor fitting for Hack's law exponent ($r^2 < 0.75$), the minimum *h* increased to 0.28 (Fig. 3c). These excluded basins (n=156) are located in generally flat topography, including some small crater basins. The mean *h* value of the remaining basins (n=2406) is 0.50, which is slightly lower than the mean value of 0.54 for the US, and majority of values are between 0.4 and 0.6. The mean Martian value is closest to that of the mean values of cold spots (0.48) and arid area (0.50) in the US (Table S1).

Spatial autocorrelation analysis (Global Moran's I) of *h* on Mars with the same null hypothesis (that the spatial distribution of *h* is random) generated a Moran's Index of 0.050, a z-score of 10.891089 and p-value of <0.0001, which also indicates that the spatial distribution is clustered and the null hypothesis can be safely rejected (ESRI, n.d.-a). This result suggests that the processes responsible for the VN formation on Mars were not random.

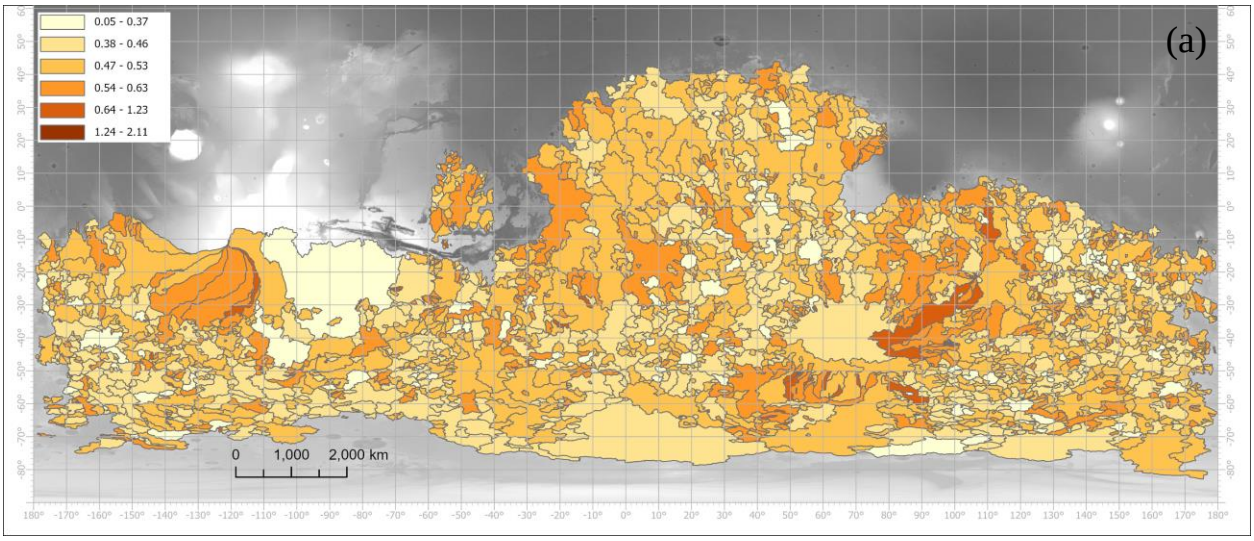

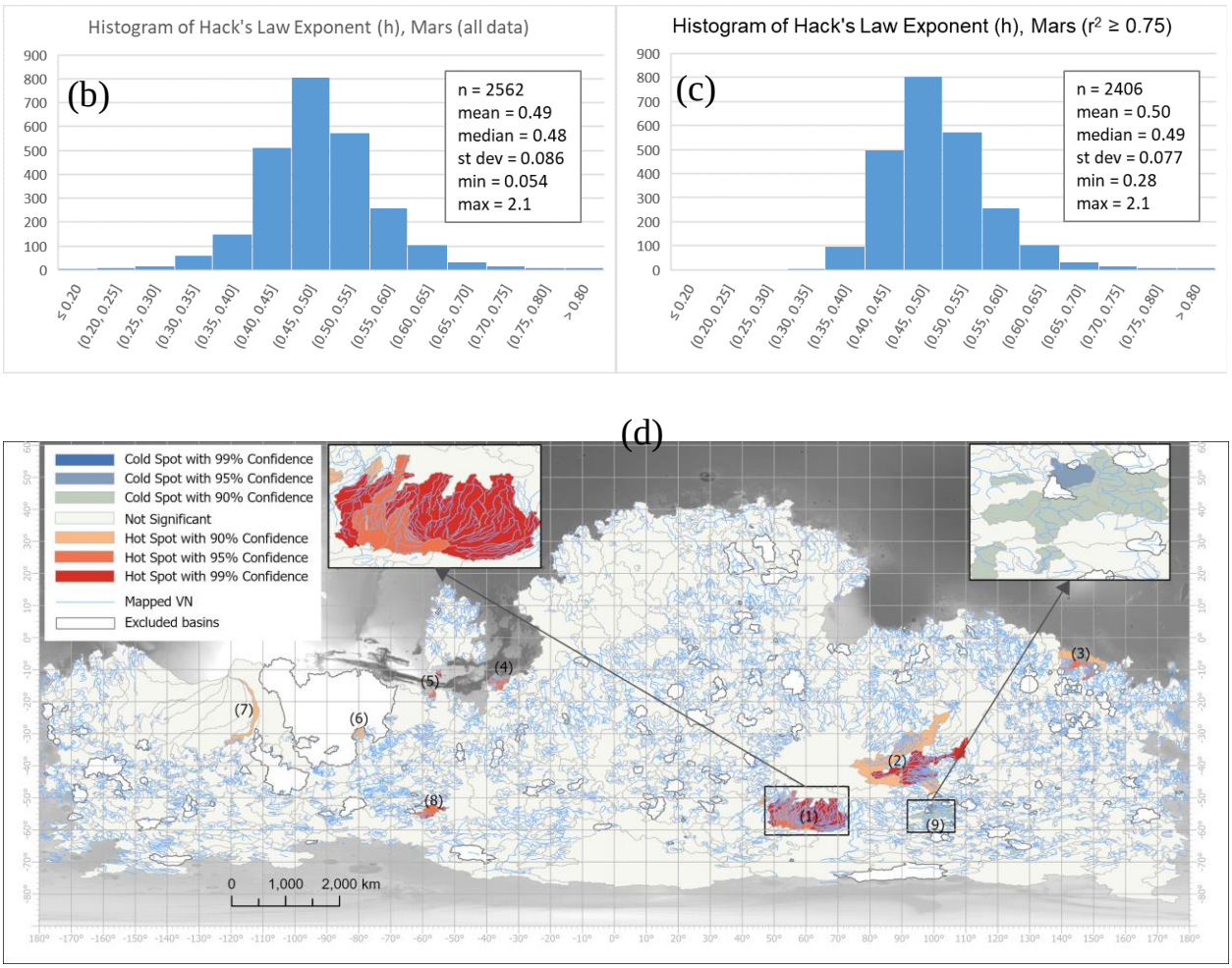

Figure 3. (a) Spatial distribution of Hack's Law exponent *h* (note: *h* is derived from 200 m resolution blended MOLA-HRSC DEM). (b) Histogram of all *h*. (c) Histogram of *h* with $r^2 \geq 0.75$. (d) Hot spot analysis of *h*. See text for more details.

We also conducted a similar Optimized Hot Spot Analysis (Getis-Ord Gi*) (ESRI, n.d.-b) as we did for US. The result is shown in Fig. 3d. A more detailed description of our observation of hotspots can be found in Supplement Material 3. Overall, these high value areas are related to the underlying topography and appear to be influenced by planar surfaces of volcanic lava flows and structures. This is similar to the nearly parallel streams developed in the exposed lakebed plain on the south shore of Lake Superior in Ontonagon, Michigan, which followed the previous glacial grooves that extended downslope toward the lake (with h = 0.6) (Hack, 1965). Another Earth analog is the shallowly-incised drainage on Hawaiian volcanoes (particularly the northeastern slopes of Mauna Kea and the Kohala peninsula, Big Island, Fig. S7). The mean *h* value of the Mars hotspots is 0.57, which is similar to that of hotspots on Earth (0.64) and that of Ontonagon, Michigan (0.6) and northeastern slopes Hawaii Big Island (0.57).

The only cold spot (blue) area is located southeast of the Hellas Basin, mostly in Early, Middle, and Late Noachian highland units and massif unit (eNh, mNh, lNh, eNhm) (Tanaka et al., 2014). The mapped VNs here appear poorly developed and non-dendritic (Fig. 4d inset), which

may also be the result of strong post-formational degradation by mid-latitude ice/glacial activities and/or dust accumulation.

The statistics of *h* values of all basins and different categories of hot/cold spots are summarized in Table S1. The majority of the Martian basins are in the non-hot/cold spots category with mean and median *h* values of 0.49, similar to those of arid area and cold spots on in the US (0.48-0.5) (Table S1). The standard deviation values of *h* on Mars in all categories are small and comparable with their terrestrial counterparts (Tables S1). One signature of *h* value for fluvial systems on Earth is that it clusters tightly around 0.5-0.6. The facts that there is widespread spatial distribution of *h* on Mars with value similar to arid climate on Earth and with small standard deviation comparable to terrestrial values (Fig. S6) and that the processes responsible for VN formation were not random based on spatial autocorrelation analysis suggest Martian VNs were likely formed in arid climate by fluvial runoff processes. This interpretation also suggests that runoff water is likely sourced from spatially uniform precipitation, as opposed to a spatially nonuniform source (e.g., melting ice), which would not lead to the observed pattern.

4 Summary and Discussion

We innovatively adapted a parameter-free method (IPBA) to extract watershed boundary on Mars. The only inputs required are the mapped VNs and DEM. This method overcame many of the drawbacks of flow-based method in delineating watersheds on Mars and allowed us to conduct a global scale analysis of Hack's law exponent (*h*) on Mars and to reveal large scale patterns that were not possible before. To help us better understand and interpret the meaning of *h* and its spatial pattern on Mars, we also conducted similar analysis on Earth (using primarily conterminous US as an example).

For both planets, the spatial autocorrelation analysis results show that the underlying processes leading to the spatial pattern of *h* were not random. The hot spot analysis revealed statistically significant high values (hot spots) and low values (cold spots) that are spatially clustered in certain locations. These clusters of high/low values can be explained by local conditions as discussed previously. For the US, the cold spots of *h* are related to the arid climate and/or basin and range structure. The hot spots of *h* are elongated watersheds likely caused by the fluvial erosion of long, sloping surfaces (e.g., the Pleistocene incision of the Great Plains sedimentary deposits) in humid environments. Similarly, the spatially clustered high values (hot spots) of *h* on Mars are likely related to the underlying topography and possibly influenced by planar surfaces of volcanic lava flows and structures, similar to northeastern side of Big Island, Hawaii, where the long, sloping surfaces of lava flows that were emplaced on the eastern slopes of the Kohala shield volcano produced unusually long, parallel valleys and elongated basins. The mean *h* value of these hot spots on Mars (0.57) are even slightly higher than humid areas on Earth (0.54) but less than the hot spots on Earth (0.64) (Table S1). The spatially clustered low values (cold spots) of *h* are limited to an area SE of the Hellas basin, where the VNs were poorly developed or poorly preserved perhaps due to post-formational modification such as glacial activities.

The vast majority of the basins on Mars show no apparent spatial clustering, which means that the vast majority of the basins (2301 out of 2406 or 95.6%) have *h* values similar to those of their neighbors with a mean of 0.49 and a small standard deviation of 0.075. The mean and standard deviation values of *h* on Mars that are very similar to those of arid area and cold spots in the US strongly suggest that the early Mars climate under which VNs were generated was warm and arid. Since the tight *h* value is a signature of fluvial systems on Earth (e.g., Hack, 1957; Penido et al., 2013; Rigon et al., 1993), the small and comparable standard deviation values of the two planets indicate that runoff processes are most likely responsible for Martian VN formation. Although some structural control or impact cratering may have frustrated the full development of fluvial systems, contributing to the overall lower *h* value on Mars, they alone cannot explain the widespread distribution of low *h* value with small standard deviation across the whole planet, which can be best explained by a global arid climate condition. This spatial pattern is also consistent with runoff water sourced from spatially uniform precipitation; a spatially nonuniform source would not generate the observed pattern.

Previous studies of *h* on Mars generated values with large variabilities, likely due to the different resolutions of the data and methodologies used to extract watershed boundaries and derive *h* values. We used the same methodology for both Earth and Mars, resulting in comparable *h* values with very small standard deviations. Our new results indicate that the majority of the Mars VNs system are most likely produced by runoff processes in a warm and arid climate with enough precipitation to carve the VNs. This interpretation is consistent with a number of other recent geomorphic studies (e.g., Cang & Luo, 2019; Seybold et al., 2018) and climate models (e.g., Kamada et al., 2021; Ramirez et al., 2020).

Acknowledgments

There is no real or perceived financial conflicts of interests for any author. We acknowledge funding from NASA MDAP (80NSSC21K1087 to WL, AH, and RC and 80NSSC17K0454 to RC) and Edson Queiroz Foundation (to EO and RP). We thank Yaxiong Shao and Jichao Fang for help with data processing and 3 anonymous reviewers and Vic Baker (and Lin Ji and Tao Liu) for their reviews of earlier versions of the paper.

Open Research

Almost all data used in this study are publically available. The HydroSHEDS core dataset is available at https://www.hydrosheds.org/hydrosheds-core-downloads. The US major streams data is available from the US National Weather Service at https://www.weather.gov/gis/Rivers. The Global Aridity Index and Potential Evapotranspiration Climate Database is available at https://doi.org/10.6084/m9.figshare.7504448.v4. MOLA DEM at 463 m resolution can be downloaded at https://astrogeology.usgs.gov/search/map/Mars/GlobalSurveyor/MOLA/Mars_MGS_MOLA_D

363 EM_mosaic_global_463m. The HRSC and MOLA Blended Digital Elevation Model at 200 m is
364 available at
365 https://astrogeology.usgs.gov/search/map/Mars/Topography/HRSC_MOLA_Blend/Mars_HRSC
366 _MOLA_BlendDEM_Global_200mp_v2. The mapped VN data is from a previous publication
367 (Matsubara et al., 2013).
368

369 The IPBA software code is available on GitHub (https://github.com/erneson/IPBA). The
370 Mars watershed boundary shapefile data derived from IPBA is in the process of being archived in
371 Zenodo (https://zenodo.org/) and a copy is temporarily uploaded as Supporting Information for
372 review purposes.
373
374

375

376
377 **References**

378 Ansan, V., & Mangold, N. (2013). 3D morphometry of valley networks on Mars from
379 HRSC/MEX DEMs: Implications for climatic evolution through time. *Journal of*
380 *Geophysical Research: Planets, 118*(9), 1873–1894. https://doi.org/10.1002/jgre.20117

381 Baker, V. R., Hamilton, C. W., Burr, D. M., Gulick, V. C., Komatsu, G., Luo, W., et al. (2015).
382 Fluvial geomorphology on Earth-like planetary surfaces: A review. *Geomorphology*, *245*,
383 149–182. https://doi.org/10.1016/j.geomorph.2015.05.002

384 Buffo, J. J., Ojha, L., Meyer, C. R., Ferrier, K. L., & Palucis, M. C. (2022). Revisiting subglacial
385 hydrology as an origin for Mars' valley networks. *Earth and Planetary Science Letters*,
386 *594*, 117699. https://doi.org/10.1016/j.epsl.2022.117699

387 Cang, X., & Luo, W. (2019). Noachian climatic conditions on Mars inferred from valley network
388 junction angles. *Earth and Planetary Science Letters*, *526*, 115768.
389 https://doi.org/10.1016/j.epsl.2019.115768

Caprarelli, G., & Wang, B. Y. (2012). Wet Mars implications of revised scaling calculations for Evros Vallis. *Australian Journal of Earth Sciences*, *59*(2), 263–276. https://doi.org/10.1080/08120099.2012.622294

Craddock, R. A., & Howard, A. D. (2002). The case for rainfall on a warm, wet early Mars. *Journal of Geophysical Research*, *107(E11)*, Doi:10.1029/2001je001505.

Dodds, P. S., & Rothman, D. H. (2000). Scaling, Universality, and Geomorphology. *Annual Review of Earth and Planetary Sciences*, *28*(1), 571–610. https://doi.org/10.1146/annurev.earth.28.1.571

Ehlmann, B. L., Mustard, J. F., Murchie, S. L., Bibring, J.-P., Meunier, A., Fraeman, A. A., & Langevin, Y. (2011). Subsurface water and clay mineral formation during the early history of Mars. *Nature*, *479*(7371), 53–60. https://doi.org/10.1038/nature10582

ESRI. (n.d.-a). ArcGIS Pro: Spatial Autocorrelation (Global Moran's I) (Spatial Statistics)(https://pro.arcgis.com/en/pro-app/latest/tool-reference/spatial-statistics/spatial-autocorrelation.htm). ESRI. Retrieved from https://pro.arcgis.com/en/pro-app/latest/tool-reference/spatial-statistics/spatial-autocorrelation.htm

ESRI. (n.d.-b). How Optimized Hot Spot Analysis works (https://pro.arcgis.com/en/pro-app/latest/tool-reference/spatial-statistics/how-optimized-hot-spot-analysis-works.htm). ESRI. Retrieved from https://pro.arcgis.com/en/pro-app/latest/tool-reference/spatial-statistics/hot-spot-analysis.htm

Fastook, J. L., & Head, J. W. (2015). Glaciation in the Late Noachian Icy Highlands: Ice accumulation, distribution, flow rates, basal melting, and top-down melting rates and patterns. *Planetary and Space Science*, *106*, 82–98. https://doi.org/10.1016/j.pss.2014.11.028

Fehr, E., Andrade Jr, J. S., da Cunha, S. D., da Silva, L. R., Herrmann, H. J., Kadau, D., et al. (2009). New efficient methods for calculating watersheds. *Journal of Statistical Mechanics: Theory and Experiment*, *2009*(09), P09007. https://doi.org/10.1088/1742-5468/2009/09/P09007

Fergason, R. L., Hare, T. M., & Laura, J. (2018). HRSC and MOLA Blended Digital Elevation Model at 200m v2. Retrieved from http://bit.ly/HRSC_MOLA_Blend_v0

Forget, F., Wordsworth, R., Millour, E., Madeleine, J.-B., Kerber, L., Leconte, J., et al. (2013). 3D modelling of the early martian climate under a denser CO2 atmosphere: Temperatures and CO2 ice clouds. *Icarus*, *222*(1), 81–99. https://doi.org/10.1016/j.icarus.2012.10.019

Gough, D. O. (1981). Solar interior structure and luminosity variations. *Solar Physics*, *74*(1), 21–34. https://doi.org/10.1007/BF00151270

Grau Galofre, A., Jellinek, A. M., & Osinski, G. R. (2020). Valley formation on early Mars by subglacial and fluvial erosion. *Nature Geoscience*, *13*(10), 663–668. https://doi.org/10.1038/s41561-020-0618-x

Grau Galofre, A., Whipple, K. X., Christensen, P. R., & Conway, S. J. (2022). Valley Networks and the Record of Glaciation on Ancient Mars. *Geophysical Research Letters*, *49*(14). https://doi.org/10.1029/2022GL097974

Gulick, V. C. (1998). Magmatic intrusions and a hydrothermal origin for fluvial valleys on Mars. *Journal of Geophysical Research*, *103*, 19,365-19,387.

Hack, J. T. (1957). *Studies of longitudinal stream profiles in Virginia and Maryland*. Washington 25, D. C.: United States Geological Survey. Retrieved from https://pubs.usgs.gov/pp/0294b/report.pdf

435 Hack, J. T. (1965). *Postglacial drainage evolution and stream geometry in the Ontonagon area,*
436 *Michigan* (Professional Paper No. 504- B).
437 Halevy, I., & Head, J. W. (2014). Episodic warming of early Mars by punctuated volcanism.
438 *Nature Geoscience*, *7*(12), 865–868. https://doi.org/10.1038/ngeo2293
439 Hunt, C. B. (1967). *Physiography of the United States*. San Francisco: W.H. Freeman.
440 Hynek, B. M., & Phillips, R. J. (2003). New data reveal mature, integrated drainage systems on
441 Mars indicative of past precipitation. *Geology*, *31*, 757–760.
442 Kamada, A., Kuroda, T., Kasaba, Y., Terada, N., & Nakagawa, H. (2021). Global climate and
443 river transport simulations of early Mars around the Noachian and Hesperian boundary.
444 *Icarus*, *368*, 114618. https://doi.org/10.1016/j.icarus.2021.114618
445 Luo, W., & Stepinski, T. F. (2009). Computer-generated global map of valley networks on Mars.
446 *Journal of Geophysical Research-Planets*, *114*.
447 Mangold, N., Quantin, C., Ansan, V., Delacourt, C., & Allemand, P. (2004). Evidence for
448 Precipitation on Mars from Dendritic Valleys in the Valles Marineris Area. *Science*,
449 *305*(5680), 78–81. https://doi.org/10.1126/science.1097549
450 Matsubara, Y., Howard, A. D., & Gochenour, J. P. (2013). Hydrology of early Mars: Valley
451 network incision. *Journal of Geophysical Research: Planets*, *118*(6), 1365–1387.
452 https://doi.org/10.1002/jgre.20081
453 Mest, S. C., Crown, D. A., & Harbert, W. (2010). Watershed modeling in the Tyrrhena Terra
454 region of Mars. *Journal of Geophysical Research*, *115*(E9).
455 https://doi.org/10.1029/2009JE003429

O'Callaghan, J. F., & Mark, D. M. (1984). The extraction of drainage networks from digital elevation data. *Computer Vision, Graphics, and Image Processing*, *28*(3), 323–344. https://doi.org/10.1016/S0734-189X(84)80011-0

Oliveira, E. A., Pires, R. S., Oliveira, R. S., Furtado, V., Herrmann, H. J., & Andrade, J. S. (2019). A universal approach for drainage basins. *Scientific Reports*, *9*(1), 9845. https://doi.org/10.1038/s41598-019-46165-0

Penido, J. C., Fassett, C. I., & Som, S. M. (2013). Scaling relationships and concavity of small valley networks on Mars. *Planetary and Space Science*, *75*, 105–116. https://doi.org/10.1016/j.pss.2012.09.009

Ramirez, R. M., & Craddock, R. A. (2018). The geological and climatological case for a warmer and wetter early Mars. *Nature Geoscience*, *11*(4), 230–237. https://doi.org/10.1038/s41561-018-0093-9

Ramirez, R. M., Craddock, R. A., & Usui, T. (2020). Climate Simulations of Early Mars With Estimated Precipitation, Runoff, and Erosion Rates. *Journal of Geophysical Research: Planets*, *125*(3). https://doi.org/10.1029/2019JE006160

Rigon, R., Rinaldo, A., Rodriguez-Iturbe, I., Bras, R. L., & Ijjasz-Vasquez, E. (1993). Optimal channel networks: A framework for the study of river basin morphology. *Water Resources Research*, *29*(6), 1635–1646. https://doi.org/10.1029/92WR02985

Seybold, H. J., Kite, E., & Kirchner, J. W. (2018). Branching geometry of valley networks on Mars and Earth and its implications for early Martian climate. *Science Advances*, *4*(6), eaar6692. https://doi.org/10.1126/sciadv.aar6692

Smith, D. E., Zuber, M. T., Frey, H. V., Garvin, J. B., Head, J. W., Muhleman, D. O., et al. (2001). Mars Orbiter Laser Altimeter: Experiment summary after the first year of global

mapping of Mars. *Journal of Geophysical Research: Planets*, *106*(E10), 23689–23722. https://doi.org/10.1029/2000JE001364

Som, S. M., Montgomery, D. R., & Greenberg, H. M. (2009). Scaling relations for large Martian valleys. *Journal of Geophysical Research*, *114*(E2). https://doi.org/10.1029/2008JE003132

Stepinski, T. F., & Coradetti, S. (2004). Comparing morphologies of drainage basins on Mars and Earth using integral-geometry and neural maps (DOI 10 1029/2004GLO20359). *GEOPHYSICAL RESEARCH LETTERS*, *31*, n.

Tanaka, K. L., Skinner, J. A. Jr., Dohm, J. M., Irwin, R. P., III, Kolb, E. J., Fortezzo, C. M., et al. (2014). *Geologic map of Mars: U.S. Geological Survey Scientific Investigations Map 3292, scale 1:20,000,000*.

Trabucco, A., & Zomer, R. (2022). Global Aridity Index and Potential Evapotranspiration (ET0) Climate Database v3 [Data set]. figshare. https://doi.org/10.6084/M9.FIGSHARE.7504448.V4

Turbet, M., & Forget, F. (2019). The paradoxes of the Late Hesperian Mars ocean. *Scientific Reports*, *9*(1). https://doi.org/10.1038/s41598-019-42030-2

UNEP, (United Nations Environment Programme). (1997). World Atlas of Desertification: Second Edition. Retrieved from https://wedocs.unep.org/20.500.11822/30300

Vincent, L., & Soille, P. (1991). Watersheds in digital spaces: an efficient algorithm based on immersion simulations. *IEEE Transactions on Pattern Analysis and Machine Intelligence*, *13*(6), 583–598. https://doi.org/10.1109/34.87344

Wilkinson, D., & Willemsen, J. F. (1983). Invasion percolation: a new form of percolation theory. *Journal of Physics A: Mathematical and General*, *16*(14), 3365–3376. https://doi.org/10.1088/0305-4470/16/14/028

Wordsworth, R. D. (2016). The Climate of Early Mars. *Annual Review of Earth and Planetary Sciences*, *44*(1), 381–408. https://doi.org/10.1146/annurev-earth-060115-012355

Wordsworth, R. D., Forget, F., Millour, E., Head, J. W., Madeleine, J.-B., & Charnay, B. (2013). Global modelling of the early martian climate under a denser CO2 atmosphere: Water cycle and ice evolution. *Icarus*, *222*(1), 1–19. https://doi.org/10.1016/j.icarus.2012.09.036

Yi, R. S., Arredondo, Á., Stansifer, E., Seybold, H., & Rothman, D. H. (2018). Shapes of river networks. *Proceedings of the Royal Society A: Mathematical, Physical and Engineering Sciences*, *474*(2215), 20180081. https://doi.org/10.1098/rspa.2018.0081